Environmental Science & Technology

Article

pubs.acs.org/est

Speciation of Arsenic, Chromium, and Vanadium in Red Mud Samples from the Ajka Spill Site, Hungary

Ian T. Burke,*[,†] William M. Mayes,[‡] Caroline L. Peacock,[†] Andrew P. Brown,[§] Adam P. Jarvis,[∥] and Katalin Gruiz[⊥]

[†]Earth Surface Science Institute, School of Earth and Environment, University of Leeds, Leeds LS2 9JT, U.K.

[‡]Centre for Environmental and Marine Sciences, University of Hull, Scarborough, YO11 3AZ, U.K.

[§]School of Process, Environmental and Materials Engineering, University of Leeds, Leeds LS2 9JT, U.K.

[∥]School of Civil Engineering and Geosciences, Newcastle University, Newcastle upon Tyne, NE1 7RU, U.K.

[⊥]Department of Applied Biotechnology and Food Science, Budapest University of Technology and Economics, 1111 Budapest, St. Gellért sq. 4, Hungary

Supporting Information

ABSTRACT: Results are presented from X-ray absorption spectroscopy based analysis of As, Cr, and V speciation within samples of bauxite ore processing residue (red mud) collected from the spill site at Ajka, Western Hungary. Cr K-edge XANES analysis found that Cr is present as Cr^{3+} substituted into hematite, consistent with TEM analysis. V K-edge XANES spectra have $E_{1/2}$ position and pre-edge features consistent with the presence of V^{5+} species, possibly associated with Ca-aluminosilicate phases. As K-edge XANES spectra identified As present as As^{5+}. EXAFS analysis reveals arsenate phases in red mud samples. When alkaline leachate from the spill site is neutralized with HCl, 94% As and 71% V are removed from solution during the formation of amorphous Al-oxyhydroxide. EXAFS analysis of As in this precipitate reveals the presence of arsenate Al-oxyhydroxide surface complexes. These results suggest that in the circumneutral pH, oxic conditions found in the Torna and Upper Marcal catchments, incorporation and sorption, respectively, will restrict the environmental mobility of Cr and As. V is inefficiently removed from solution by neutralization, therefore, the red mud may act as a source of mobile V^{5+} where the red mud deposits are not removed from affected land.

INTRODUCTION

Red mud is the fine material byproduct of Al-extraction from bauxite via the Bayer processes, and up to 120 million tonnes are produced annually.[1] Although in recent years there have been multiple attempts to find practical uses for red mud (e.g., in water decontamination,[2,3] soil conditioning,[4] and CO_2 sequestration[5]) the majority of red mud produced is stored in land based depositories[1,6] or has been dumped into the sea.[7] To prevent dust formation, red mud is often stored as wet slurry, and once filled, depositories are covered and revegetated to cap the waste.[8,9]

The failure of the northwestern corner of Cell X of the Ajkai Timfoldgyar Zrt alumina plant red mud depository (Western Hungary) on October 4, 2010 resulted in the release of ∼1 million m^3 of caustic metalliferous red mud suspension.[10,11] Cell X was the active depository in use at the time, therefore, it contained red mud suspension with high water content (solids ∼200−300 g L^{-1})[10] promoting the long-range transport of the released material. The waste inundated homes and land downstream killing 10 persons and causing over 100 other serious injuries.[9,12] Approximately 40 km^2 of agricultural and urban land was affected and the red mud was transported over 120 km downstream by rivers reaching the Danube itself.[9,11]

The specific composition of red mud is highly dependent on the nature of the bauxite used. Red mud typically comprises residual iron oxides, quartz, sodium aluminosilicates, titanium dioxide, calcium carbonate/aluminate, and sodium hydroxide (which raises the pH up to 13).[6,9,13,14] Associated red mud leachates are also hyperalkaline (up to pH ∼13), which itself can be directly toxic to aquatic life.[15] Equally important is the greater mobility of oxyanionic forming trace elements such as As, Cr, and V at elevated pH.[16] At Ajka, water in the highly alkaline (pH 13) red mud suspension has elevated concentrations of metals and metalloids such as Al (650 ppm), As, V, and Mo (4−6 ppm), and the red mud itself has elevated concentrations of As, V, Cr, Co, and Ni (100−1000 ppm).[12,17]

Within days after the spill, acid dosing of surface waters was established close to the impoundment breach[17] and was

Received: September 13, 2011
Revised: February 10, 2012
Accepted: February 11, 2012
Published: February 13, 2012

   dx.doi.org/10.1021/es3003475 | Environ. Sci. Technol. 2012, 46, 3085−3092

effective in lowering both pH values and metal(loid) concentrations immediately downstream of the spill.[11,17] Gypsum ($CaSO_4{\cdot}2H_2O$) addition was also extensively used to lower pH at sites from 5 to 70 km downstream.[17,18] Mixing of the red mud with soils, river sediments, and uncontaminated surface water also contributed to the overall pH reductions observed. Sequential extractions performed on these neutralized (pH 8−8.5), transported red mud deposits determined that the majority of metal(loids) such as As, Cr, and V (70−90%) are present in residual hard-to-leach phases.[17] The remaining 10−30% of these metal(loids), however, occurred in weak acid/hydroxylamine HCl leached phases, which may represent the presence of metal(loid) containing phases that are more environmentally available.[17] Investigation of red mud behavior in affected rivers also suggested the fine grained nature of the red mud will facilitate its downstream transport, potentially spreading contamination, but also diluting its effects.[17]

Another part of the response to the disaster was to remove the red mud from residential areas and fields (in some cases thin deposits were plowed into underlying soils) to prevent dust formation.[9,12,17] Initial investigations, however, suggested that the likely health effects from red mud derived dusts are no greater than other urban dust sources.[9,19] In red mud affected soils, the effects of elevated salinity and alkalinity were highlighted as being more important constraints on plant growth than the heavy metal content.[12] Despite these initial findings, the longer term behavior and potential mobility of metal(loids) in neutral red mud affected environments are still largely unknown. Indeed, Grafe et al.[13] recently highlighted limited knowledge of trace metal speciation and leaching behavior as a key knowledge gap in relation to the management of bauxite residues.

This study had the following specific objectives: (1) X-ray absorption spectroscopy analysis was combined with electron microscopy to determine As, Cr, and V speciation within the red mud. (2) Alkaline leachate associated with the red mud was acid neutralized, the changes in metal(loid) concentrations were determined, and the speciation of As and V in the neoformed leachate precipitate was investigated. (3) This new information was used in conjunction with published data[12,17] to predict the likely environmental mobility, fate, and long-term hazards from As, Cr, and V contamination associated with the red mud spill.

MATERIALS AND METHODS

Field Sampling and Sample Handling. In December 2010 triplicate samples of red mud (K1a, K1b, and K1c) were recovered from the dyke breach of the Ajka red mud impoundment (Location K1 in 17; Lat 47°05′20 N, Long 14°29′43 E). The samples were air-dried, disaggregated using a mortar and pestle, and sieved to retain the <2 mm fraction. Red mud leachate was collected from a leachate drain at location K1 and stored at 5 °C in polypropylene bottles until used.

Leachate Neutralization Experiment. Unfiltered red mud leachate (50 mL) was neutralized to pH 8.3 (typical pH value recorded at sampling stations 5 km downstream of K1[17]) by dropwise addition of 6 mol L^{-1} HCl. The pH was determined using an Orion benchtop meter calibrated with pH 7 and pH 10 buffer solutions. Below pH 10.5 a cloudy white precipitate formed. The suspension was left to equilibrate for 13 days then centrifuged for 10 min at 6000*g*. The supernatant was removed, filtered (0.2 μm), and analyzed as below. The precipitate was washed in a pH 8.3 NaOH solution and dried at 70 °C.

Sample Characterization. Sample digestion was achieved via microwave-assisted total digestion (aqua regia and HF).[20] Elemental concentrations in digests and aqueous samples were analyzed using a Perkin-Elmer Elan DRCII inductively coupled plasma-mass spectrometer (ICP-MS; As and Cr) and an Optima 5300 DV ICP-OES (all other elements). X-ray powder diffraction (XRD) analysis of K1c red mud and the leachate precipitate was performed on a Bruker D8 Advance XRD with a Cu tube.

Transmission Electron Microscopy (TEM). Approximately 0.1 g of K1c was suspended in ethanol, placed on a Cu support grid with holey carbon support film (Agar Scientific, UK), and air-dried prior to analysis. The specimen was examined using a Philips/FEI CM200 field emission gun TEM fitted with a scanning (STEM) unit and an ultrathin window energy dispersive X-ray detector (Oxford Instruments ISIS EDX).

X-ray Absorption Spectroscopy (XAS). XANES and EXAFS data were collected at station I18 at the Diamond Light Source, UK, in April, 2011. One hundred mg of two red mud samples (K1a and K1c) and the precipitate recovered from the leachate neutralization experiment were prepared as pressed pellets for analysis. XAS spectra were collected at the As, Cr, and V K-edges (11867, 5989, and 5465 eV, respectively). Standard spectra were collected from a range of laboratory chemicals and aqueous solutions (1000 mg L^{-1}). In addition an amorphous Cr-hydroxide standard was prepared via precipitation achieved through dropwise neutralization of $CrCl_3$ solution by sodium hydroxide.[21] The resulting precipitate was then washed with distilled water to remove all impurities and dried in an oven at 60 °C for 24 h. A 5% Cr^{3+}-substituted hematite standard was prepared following the method of 22 and Cr K-edge XANES spectra were collected at the SuperXAS beamline of the Swiss Light Source. All XANES and EXAFS spectra were summed and normalized using Athena v0.8.061 and XANES data were plotted for samples and standards. Cr and V K-edge spectra from red mud samples were affected by irresolvable interferences with Nd and La L_3-edges observed at 6208 and 5483 eV respectively, therefore, EXAFS spectra were not analyzed. As K-edge spectra from all samples were interference free and background subtraction for EXAFS analysis was performed using PySpline v1.1. Background subtracted EXAFS spectra were then fit in DLexcurv v1.0[23] to model clusters representing various As binding environments relevant to the red mud and the precipitate recovered from the leachate neutralization experiment (Supporting Information Figure SI 1). Multiple scattering was allowed for as coded in Dlexcurv v1.0.[23,24] Improvement in *R* value (as coded in 24) was used as a measure of goodness of fit. In addition, reduced Chi^2 values were used to evaluate fits of each experimental spectrum to various single shell vs multiple shell model clusters (see SI, Sections 1 and 2 for detailed descriptions and protocols).

RESULTS

Sample Characterization. XRD analysis of the red mud revealed hematite (Fe_2O_3), calcite ($CaCO_3$), cancrinite ($Na_6CaAl_6Si_6(CO_3)O_{24}{\cdot}2H_2O$), and hydrogarnet ($Ca_3AlFe(SiO_4)(OH)_8$), with minor amounts of boehmite (AlO(OH)) and gibbsite ($Al(OH)_3$), similar to previous analysis of deposited red mud samples but without any soil and sediment derived minerals.[9] The precipitate formed during leachate neutralization was amorphous by X-ray diffraction, similar to previous reports of precipitates formed from Al-rich leachates.[25] Leachate neutralization is very effective in removing soluble Al (99.7% removed), As, B, Fe, Ga, Ni, and Si (85−94% removed),

but is progressively less effective in removing soluble Pb (78% removed), Cu (77% removed), V (71% removed), Mo (47% removed), and Cr (26% removed) (Table 1). The ranges of

Table 1. Concentration of Selected Soluble Elements in Red Mud Leachate and Neutralized Leachate (0.2-μm Filtered)

determinand	red mud leachate	neutralized leachate	% removed
pH	12.6	8.3	
selected elements (μg L^{-1})			
Al	833500	2400	99.7
As	6325	383	93.9
B	1693	107	93.7
Cr	65	48	26.0
Cu	429	100	76.6
Fe	288	<10[a]	>96.5
Ga	3820	294	92
Mo	7883	4190	46.9
Ni	35	5	85.1
Pb	405	89	77.8
Si	9133	642	93.0
V	8977	2650	70.5

[a]Less than given limit of detection.

As, Cr, and V concentrations in K1 red mud samples are 37−110, 733−934, and 860−963 mg kg^{-1}, respectively (see SI Table SI 1 for the total major and minor element composition of replicates K1a, K1b, and K1c). Samples K1a and K1c were selected for detailed XAS analysis due to their higher concentrations of As, Cr, and V.

TEM Analysis. Figure 1a shows an aggregate of small particles typical of red mud from the Ajka spill.[9,17] The fine

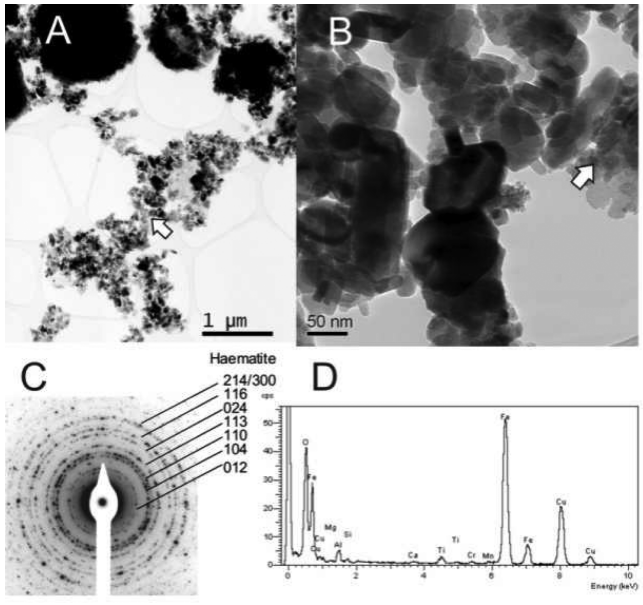

Figure 1. (A) Low-resolution bright field (S)TEM image of K1c red mud particles. (B) Higher magnification image of area highlighted by white arrow in A. (C) Selected area electron diffraction pattern with the polycrystalline rings labeled by hematite miller indices; and (D) EDX spectra collected from the point shown with a white arrow in B.

matrix particles (Figure 1b) are identified by selected area electron diffraction (SAED) (Figure 1c) as aggregates of crystalline hematite particles typically 10−200 nm in size (although areas with <5 nm particles also occur (SI Figure SI 2)). EDX analysis of hematite particles (Figure 1d) contained large peaks due to the presence of Fe and O with smaller peaks for Al, Ti, Si, Ca, Cr, and Mn (Cu peaks are due to the TEM support grid). SAED analysis of larger 1−2 μm plate-like crystals was impossible due to rapid beam damage. EDX analysis, however, revealed distinct Na−Al−Si rich and Ca−Al−Si rich compositions consistent with the cancrinite- and hydrogarnet-like phases already identified by XRD in the same sample. V peaks were found to be present in EDX spectra collected from the Ca−Al−Si rich hydrogarnet-like phase only (SI Figure SI 3−4). (The energy of the Ti K_β and V K_α peaks overlap in EDX spectra, therefore, the presence of V in these particles was indicated by the presence of the V K_β peak.)

Chromium XANES Analysis. The Cr K-edge XANES spectrum from red mud sample K1a lacks the large characteristic pre-edge peak associated with Cr^{6+} at 5993 eV and has its main absorption edge at position similar to the CrOOH and Cr_2O_3 standards (Figure 2). This indicates that the majority of

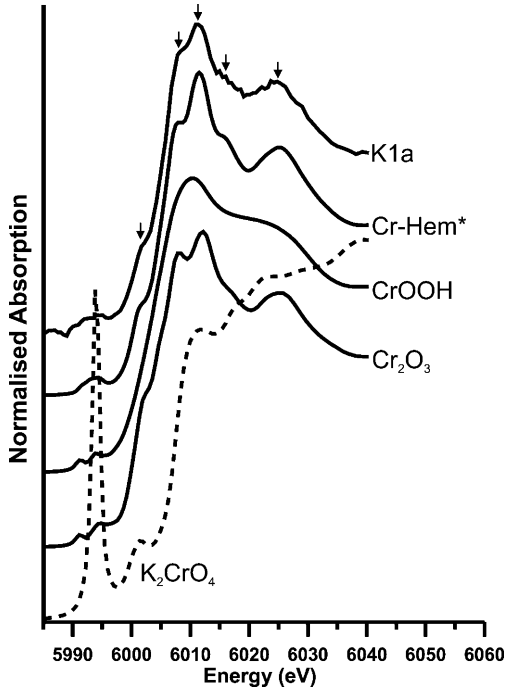

Figure 2. Normalized Cr K-edge XANES spectra collected from the red mud sample K1a and three Cr(III) and one Cr(VI) containing standards. Arrows mark position of spectral features discussed in text. *E_0 for the Cr-hematite spectrum was shifted +1.2 eV to match the Cr_2O_3 spectra.

Cr is present as Cr^{3+}. The red mud spectrum contains features consisting of sub peaks and shoulders throughout the XANES region (marked by arrows in Figure 2) that resemble XANES spectra collected from the Cr^{3+}-substituted hematite and Cr_2O_3 standards.

Arsenic XANES Analysis. The As K-edge XANES spectra (Figure 3) collected from both red mud samples (K1a and K1c) and the leachate precipitate all have their edge position and white line peaks at the same energy as the arsenate standard. This indicates that the majority of As is present as As^{5+} in all samples. All samples also have a small shoulder on the absorption edge at the same energy as the arsenite standard peak that is absent in the arsenate standard. This indicates that some As^{3+} is also present; however, linear combination fitting

dx.doi.org/10.1021/es3003475 | Environ. Sci. Technol. 2012, 46, 3085−3092

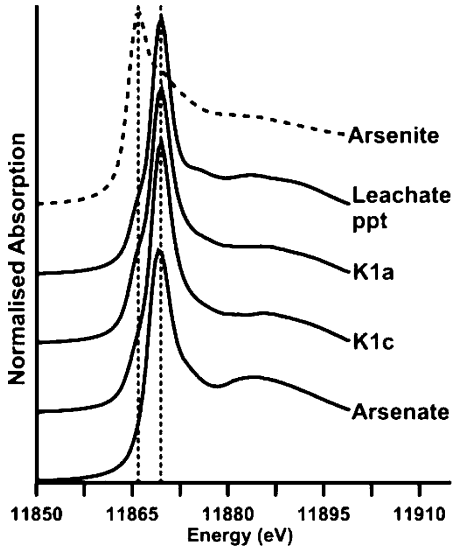

Figure 3. Normalized As K-edge XANES spectra collected from red mud samples (K1a and K1c), the K1 leachate precipitate, and 1000 mg·L^{-1} arsenic standard solutions. Vertical lines should guide the eye.

using arsenate and arsenite spectra as end members suggests the As^{3+} contribution is less than 5%.

Arsenic EXAFS Analysis. Arsenic K-edge EXAFS spectra (Figure 4) collected from two red mud samples (K1a and K1c)

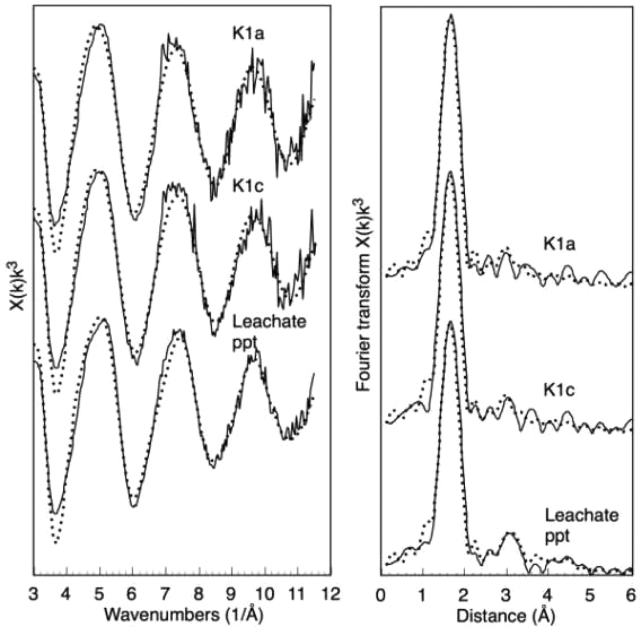

Figure 4. Right: Background subtracted As K-edge EXAFS spectra collected from red mud samples (K1a and K1c) and the K1 leachate precipitate. Left: Corresponding Fourier transforms calculated from EXAFS spectra. Dashed lines represent DLexcurv V1.0 model fits using the parameters listed in Table 2.

both have similar coordination environments with spectra fitted with 4 oxygen backscatters at 1.65−1.74 Å (Table 2). An additional peak identified in the Fourier transforms at around 2.8 Å could be entirely attributed to multiple scattering within the arsenate tetrahedron.[26] The fits to these spectra could not be statistically improved (reduced Chi^2) by including an additional shell of either Al or Fe backscatterers at ∼3.2 or

Table 2. As K-edge EXAFS Fits[a]

					goodness of fit	
sample	shell	*N*	R (Å)	$2\sigma^2$ (Å^2)	*R* (%)	reduced χ^2
K1a	O	1	1.66	0.007	22	56
	O	1	1.67	0.005		
	O	1	1.72	0.005		
	O	1	1.72	0.006		
K1c	O	1	1.63	0.005	23	56
	O	1	1.69	0.010		
	O	1	1.70	0.005		
	O	1	1.73	0.004		
leachate ppt	O	1	1.65	0.009	20	32
fit with 4 O	O	1	1.66	0.010		
	O	1	1.70	0.006		
	O	1	1.74	0.005		
leachate ppt	O	1	1.65	0.010	19	24
fit with 4 O and 2 Al	O	1	1.66	0.012		
(shown in Figure 4)	O	1	1.69	0.004		
	O	1	1.73	0.004		
	Al	1	3.19	0.015		
	Al	1	3.19	0.021		
leachate ppt	O	1	1.63	0.009	18	22
fit with 4 O and 2 Fe	O	1	1.65	0.006		
	O	1	1.71	0.005		
	O	1	1.73	0.005		
	Fe	1	3.33	0.020		
	Fe	1	3.25	0.030		

[a] *N* is the occupancy (± 25%), R is the interatomic distance (± 0.02 Å for the first shell, ± 0.05 Å for outer shells), $2\sigma^2$ is the Debye-Waller factor (± 25%), and *R* and reduced χ^2 are the least squares residual and the reduced Chi^2 goodness of fit parameters, respectively. Four As−O bonds have been considered separately to allow for multiple scattering within the AsO_4 tetrahedron. *N* values were held constant during the fitting.

3.3−3.4 Å, respectively. EXAFS data collected from the leachate precipitate were best fit with an additional shell of ∼2 Al/Fe backscatters at around 3.2 or 3.3−3.4 Å, respectively, with a resultant ∼28% improvement in reduced Chi^2 (comparing the fit with 4 oxygen backscatterers vs 4 oxygen backscatterers and 2 Al/Fe next-nearest neighbors) (Table 2).

Vanadium XANES Analysis. The V K-edge XANES spectrum (Figure 5) collected from the red mud sample K1c has a prominent pre-edge peak at 5470 eV (all energy values are quoted to ±0.25 eV) with a normalized intensity of 0.50. The main absorption edge ($E_{1/2}$ = point where absorption reaches 50% of the normalized absorption) is at 5480.3 eV. The V K-edge XANES spectrum collected from the leachate precipitate also has a pre-edge peak at 5470 eV, with a normalized intensity of 0.55 and $E_{1/2}$ = 5479.9 eV. The $E_{1/2}$ positions for standard spectra are as follows: aqueous vanadate = 5480.9 eV, V_2O_5 = 5480.4 eV, $VOSO_4{\cdot}xH_2O$ = 5479.6 eV, and V_2O_3 = 5478.5 eV.

DISCUSSION

Speciation of Chromium, Arsenic, and Vanadium in Red Mud. Cr K-edge XANES analysis reveals that Cr in red mud is predominately present as Cr^{3+}, supporting previous observations that virtually no Cr^{6+} could be extracted from red mud samples recovered downstream of the spill.[12] There is a similarity between the red mud spectra and both the Cr-substituted hematite and Cr_2O_3 standard spectra, suggesting a similar Cr^{3+} coordination environment in all three spectra. (In SI Figure SI 5, a more detailed comparison reveals a slightly

dx.doi.org/10.1021/es3003475 | Environ. Sci. Technol. 2012, 46, 3085−3092

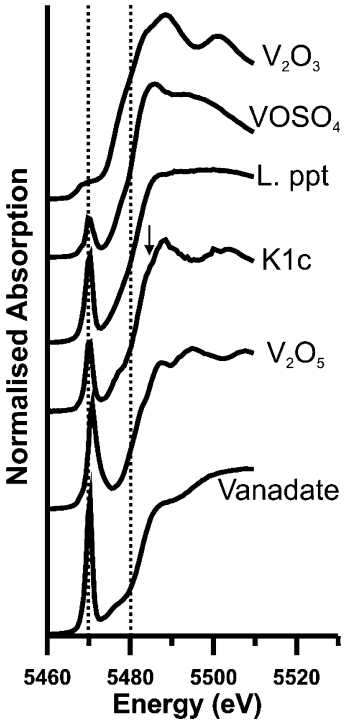

Figure 5. Normalized V K-edge XANES spectra collected from the red mud sample K1c, the leachate precipitate (L. ppt) and V^{3+}, V^{4+}, and V^{5+} containing standards. The vanadate spectrum is from a 1000 mg L^{-1} aqueous solution in 0.1 mol L^{-1} NaOH. Arrow marks position of the La L_3-edge which is superimposed onto the K1c data above this energy. Vertical lines should guide the eye.

better match to the Cr-substituted hematite standard). XANES data are complimented by TEM analyses that indicate Cr is colocalized in hematite particles (this study and 9). At the elevated pH and temperatures encountered in the Bayer Process, hematite recrystallization will be promoted,[27] and Cr^{3+} is known to readily substitute for Fe^{3+} in metal oxides.[22] Thus, incorporation into hematite is the most likely fate for Cr^{3+} in the red mud and is supported by a similar association of Cr^{3+} in iron oxide particles previously observed in μXANES analysis of Australian bauxite residues.[28]

As K-edge XANES analysis reveals that the As in red mud samples is present predominantly in the As^{5+} oxidation state. Further EXAFS analysis of spectra collected from red mud samples shows that the local coordination environment is consistent with the tetrahedral arsenate structure. There is no evidence for any contribution to these spectra from additional shells of backscattering atoms at longer distances. This chemical structure is consistent with arsenate oxyanions present as simple outer-sphere sorption complexes. Arsenate associated with iron and aluminum oxyhydroxides commonly forms inner-sphere sorption complexes, with next-nearest neighbor (second shell) features evident in the EXAFS analysis.[24,26,27] In contrast, EXAFS analysis of inorganic phases such as calcium arsenate ($Ca_3(AsO_4)_2$) and mansfieldite ($AlAsO_4{\cdot}2H_2O$) reveal no long-range structure beyond the AsO_4 tetrahedron.[29] Mineral saturation modeling (SI Table SI 3) using the K1 red mud leachate composition indicates that the solution is undersaturated with respect to a range of Ca-arsenates and Al-arsenate, but is oversaturated with respect to Ba-arsenate ($Ba_3(AsO_4)_2$), which is relatively insoluble at elevated pH.[30,31] The presence of inorganic arsenate phases in the red mud, therefore, is consistent with EXAFS and modeling results.

V K-edge XANES spectra have a reported trend in increasing absorption edge position ($E_{1/2}$) with increasing V valence state of approximately 1−2 eV per valence increase.[32,33] $E_{1/2}$ is also affected by variation in V coordination structure which can cause overlap in $E_{1/2}$ values between compounds with different V oxidation states.[33,34] $E_{1/2}$ values recorded for the red mud sample (5480.3 eV) are within the range of values reported for V^{5+} containing compounds,[32,34−36] and just below that recorded for V_2O_5 in this study. In addition, the majority of V^{4+} containing compounds reported have $E_{1/2}$ values below 5479.4 eV.[32,34,37] The normalized pre-edge peak intensity also increases with V oxidation state. The normalized pre-edge peak intensity values determined from the red mud spectra (0.50) are also within the range reported for V^{5+} compounds but there is considerable overlap with V^{4+} compounds for this indicator.[34] Likewise the energy of the pre-edge peak increases with oxidation state, but again V^{4+} and V^{5+} are not separated by this indicator.[33] Graefe et al.[28] found V present primarily as V^{4+} associated with goethite particles in a sample of Darling Range bauxite residue (Western Australia), however, goethite is absent from the Ajka red mud (this study and 9) and V was not found associated with hemeatite particles in the red mud at concentrations detectable by EDX analysis. Indeed, at the pH and Eh reported for the red mud[17] the presence of appreciable V^{4+} is not expected due to rapid oxidation to V^{5+} that is catalyzed by OH^- and mineral surfaces.[38−40] Therefore, although $E_{1/2}$, and especially pre-edge peak intensity, should be applied with care when assigning V oxidation state, it can be reasonably inferred that much of the V within the red mud sample is present as V^{5+}.

Although mineral saturation modeling results (SI Table SI 3) predict that no vanadate phase is oversaturated in the red mud leachate, the V-XANES data reported for a Ca-vanadate standard ($E_{1/2}$ = 5480 eV; pre-edge peak = 5470 eV, pre-edge peak intensity = 0.5[35]) are within error of data collected from the red mud. TEM analysis of red mud particles, however, found V associated with a Ca-aluminosilicate phase with a hydrogarnet-like composition (SI Figure S4). Hydrogarnet is known to be able to incorporate oxyanions such as chromate (CrO_4^{2-}) by substituting for four hydroxyls ($H_4O_4^{4-}$) in its structure[41] and the similar size and structure of the vanadate ion compared to chromate may also promote such substitution. Substitution of vanadate into hydrogarnet-like phases within the red mud, may therefore, limit V mobility; although the affinity and stability of V in such phases, and the nature of their V K-edge XANES spectra are unknown.

Chromium, Arsenic, and Vanadium Behavior during Leachate Neutralization. When red mud leachate is acid-neutralized a neoformed amorphous Al-rich oxyhydroxide precipitate is formed (Al concentrations are reduced from 834 to 2.4 mg L^{-1}). There is also an observed overall reduction the concentrations of the potentially hazardous trace elements present in the leachate, however, the degree of removal varied by element. For oxyanionic forming elements such as As, Cr, and V the degree of removal observed is consistent with the variation in pH-dependent sorption behavior observed for arsenate, chromate, and vanadate with metal oxyhydroxides during pH reduction (i.e., at pH 8.3 arsenate is predicted to have greater affinity for mineral surfaces than vanadate, and chromate is predicted to remain highly soluble).[16,42]

Cr concentrations in the leachate are relatively low, as was the degree of sorption to the neoformed precipitate (precluding XAS analysis of Cr speciation in this sample). Cr^{3+} is predicted

to precipitate as Cr-hydroxide at circumneutral pH, however, Cr^{6+} is predicted to be soluble as chromate throughout the circumneutral to alkaline pH range.[43] This suggests that aqueous Cr may be present as Cr^{6+} as the chromate ion. Although Cr was not strongly removed from solution during leachate neutralization, downstream dilution lowers aqueous [Cr] to undetectable concentrations in river water samples.[17]

Analysis of As K-edge EXAFS spectra collected from the leachate precipitate shows that the local coordination environment is consistent with the tetrahedral arsenate structure. There is also evidence (reduced Chi^2) for additional Fe/Al backscatterers at approximately 3.2−3.4 Å consistent with the formation of bidentate corner-sharing complexes on iron and aluminum oxyhydroxides.[26,44,45] Assuming a similar affinity of arsenate for Al and Fe oxyhydroxide surfaces, then the majority of the As is more likely to be found with the Al oxyhydroxides that dominate the leachate precipitate (Table 1). The existence of arsenate in inner-sphere surface sorption complexes associated with the neutralized precipitate also implies pH will be an important control for As mobility.[16,42] The elevated pH present in the red mud repository promoted high arsenate solubility, but soluble As is almost completely absent downstream where pH is lowered[17] and adsorption dominates.

V K-edge XANES spectra collected from the leachate precipitate also have spectral features that are consistent with the presence of vanadium in the V^{5+} oxidation state. This is not surprising as, at the pH present in the red mud repository, vanadate is predicted to dominate aqueous speciation.[39,46,47] When the leachate was neutralized, therefore, some adsorption of vanadate to the neoformed precipitate is expected.[39,42] The degree of vanadate adsorption increases as pH is lowered but complete adsorption to minerals is not observed at circumneutral pH when surface loadings are elevated.[48,49] In experiments using goethite this effect is attributed to the formation of more soluble polyvanadate species,[48] but saturation of potential sorption sites may also lead to elevated V concentrations at circumneutral pH. This is consistent with the behavior observed downstream of the spill in December 2010, where, despite the lowered pH and the effects of dilution, soluble V is present throughout the Torna and Upper Marcal catchments.[17]

Implications for Affected Environments. In the weeks after the spill, global media attention was focused on the immediate impacts to human welfare, property, and the environment. Much of the immediate concern focused on the risks posed by the elevated levels of potentially toxic trace metals in the red mud, including As, V, and Cr. This study and the work of others[9,12,17] have shown that in the case of As and Cr these risks seem overstated. Chromium is largely incorporated as Cr^{3+} in hematite and aqueous Cr is quickly diluted to below detection. As hematite is very insoluble at pH values between 2 and 14 ($pK_{sp} \approx 44$;[16]), and the oxidation kinetics observed for Cr^{3+} in the environment are very slow,[50] the future evolution of more soluble, toxic Cr^{6+} from red mud deposits is likely to be inhibited.

Arsenic solubility can be expected to be controlled by a combination of dissolution and adsorption reactions. Dissolution of arsenate-bearing phases may potentially release As to solution, but an abundance of suitable sorption surfaces in soils and sediments should ultimately limit As mobility. Indeed, arsenate sorbed to red mud has been shown to be very stable in neutral to acidic conditions.[51,52] In the near neutral pH, oxidizing, surface environments that characterize much of the effected Torna and Upper Marcal catchments, arsenate sorption behavior is more likely to be effected by the presence of other anions (e.g., phosphate and to a lesser extent bicarbonate), which compete for the same sorption sites.[53−55] Where red mud has been deposited into water-saturated marshes, however, development of reducing conditions may promote the reduction of arsenate to As^{3+} species that are predicted to be more soluble in sediment porewater at circumneutral pH.[47,56]

Although V is found as V^{5+}, exact speciation is much less assuredly assigned by XAS analysis. At circumneutral pH adsorption will be important in controlling V solubility, however this study and previous work[17] showed that neutralization is relatively inefficient in removing aqueous V, and soluble V was detected over 40 km downstream of the spill site. The dissolution of hydrogarnet during red mud neutralization[13] may also promote V release, and, similar to arsenate, anion exchange processes are also likely to be important in V leaching behavior. Due to the observed enhanced solubility of V^{5+} species at circumneutral pH, red mud deposits may be a potential source for soluble V^{5+} species until extensively leached by meteoric and surface waters. As a result we recommend that, where feasible, red mud deposits are recovered from affected environments. Where recovery is impracticable it is advisible that measures are taken to ensure pH remains at near neutral levels to minimize the mobility of toxic trace elements.

■ ASSOCIATED CONTENT

Supporting Information

Detailed XAS methods, red mud and leachate composition, mineral saturation indexes, molecular cluster diagrams, additional TEM images, EDX spectra, and XANES plots. This material is available free of charge via the Internet at http://pubs.acs.org.

■ AUTHOR INFORMATION

Corresponding Author

*E-mail: i.burke@see.leeds.ac.uk; phone: +44 113 3437532; fax: +44 113 3435259.

Notes

The authors declare no competing financial interest.

■ ACKNOWLEDGMENTS

We acknowledge funding from the UK Natural Environment Research Council (grant NE/I019468/1) and thank Diamond Light Source for access to beamline I18 (grant SP7058) that contributed to the results presented here. Thanks to Tina Geraki (Diamond Light Source) for support during synchrotron time, Lesley Neve (University of Leeds) for XRD analysis, and Bob Knight (University of Hull) for ICP analysis. We thank Maarten Nachtegaal (Paul Scherrer Institute) and Jacob Frommer (ETH Zurich) for sharing Cr K-edge XANES data. We also thank Orsolya Klebercz, Viktória Feigl, Mária Tolner, Ermese Vaszita (Budapest University of Technology and Economics), and Gyozo Jordan (Geological Institute of Hungary) for field support. István Csonki (Central Danubian Water and Environment Authority) is thanked for site access and orientation.

■ REFERENCES

(1) Power, G.; Graefe, M.; Klauber, C. Bauxite residue issues: I. Current management, disposal and storage practices. *Hydrometallurgy* **2011**, *108* (1−2), 33−45.

(2) Wang, S.; Ang, H. M.; Tade, M. O. Novel applications of red mud as coagulant, adsorbent and catalyst for environmentally benign processes. *Chemosphere* **2008**, *72* (11), 1621−1635.
(3) Niculescu, M.; Ionita, A. D.; Filipescu, L. Chromium Adsorption on Neutralized Red Mud. *Rev. Chim.* **2010**, *61* (2), 200−205.
(4) Summers, R. N.; Guise, N. R.; Smirk, D. D. Bauxite residue (red mud) increases phosphorous retention in sandy soil catchments in Western Australia. *Fert. Res.* **1993**, *34* (1), 85−94.
(5) Yadav, V. S.; Prasad, M.; Khan, J.; Amritphale, S. S.; Singh, M.; Raju, C. B. Sequestration of carbon dioxide (CO_2) using red mud. *J. Hazard. Mater.* **2010**, *176* (1−3), 1044−1050.
(6) Hind, A. R.; Bhargava, S. K.; Grocott, S. C. The surface chemistry of Bayer process solids: a review. *Colloids Surf., A* **1999**, *146* (1−3), 359−374.
(7) Liu, Y.; Naidu, R.; Ming, H. Red mud as an amendment for pollutants in solid and liquid phases. *Geoderma* **2011**, *163* (1−2), 1−12.
(8) Courtney, R. G.; Timpson, J. P. Reclamation of fine fraction bauxite processing residue (red mud) amended with coarse fraction residue and gypsum. *Water, Air Soil Pollut.* **2005**, *164* (1−4), 91−102.
(9) Gelencser, A.; Kovats, N.; Turoczi, B.; Rostasi, A.; Hoffer, A.; Imre, K.; Nyiro-Kosa, I.; Csakberenyi-Malasics, D.; Toth, A.; Czitrovszky, A.; Nagy, A.; Nagy, S.; Acs, A.; Kovacs, A.; Ferincz, A.; Hartyani, Z.; Posfai, M. The Red Mud Accident in Ajka (Hungary): Characterization and Potential Health Effects of Fugitive Dust. *Environ. Sci. Technol.* **2011**, *45* (4), 1608−1615.
(10) Adam, J.; Banvolgyi, G.; Dura, G.; Grenerczy, G.; Gubek, N.; Gutper, I.; Simon, G.; Szegfalvi, Z.; Szekacs, A.; Szepvolgyi, J.; Ujlaky, E. *The Kolontár Report. Causes and Lessons from the Red Mud Disaster*; Greens/European Free Alliance Parliamentary Group in the European Parliament and LMP - Politics Can Be Different: Budapest, 2011; p 156.
(11) Reeves, H. J.; Wealthall, G.; Younger, P. L. *Advisory Visit to the Bauxite Processing Tailings Dam near Ajka, Vesprem County, Western Hungary*; Open Report OR/11/006; British Geological Survey: Keyworth, UK, 2011.
(12) Ruyters, S.; Mertens, J.; Vassilieva, E.; Dehandschutter, B.; Poffijn, A.; Smolders, E. The Red Mud Accident in Ajka (Hungary): Plant Toxicity and Trace Metal Bioavailability in Red Mud Contaminated Soil. *Environ. Sci. Technol.* **2011**, *45* (4), 1616−1622.
(13) Grafe, M.; Power, G.; Klauber, C. Bauxite residue issues: III. Alkalinity and associated chemistry. *Hydrometallurgy* **2011**, *108* (1−2), 60−79.
(14) Somlai, J.; Jobbagy, V.; Kovacs, J.; Tarjan, S.; Kovacs, T. Radiological aspects of the usability of red mud as building material additive. *J. Hazard. Mater.* **2008**, *150* (3), 541−545.
(15) Wilkie, M. P.; Wood, C. M. The adaptations of fish to extremely alkaline environments. *Comp. Biochem. Physiol., B* **1996**, *113* (4), 665−673.
(16) Langmuir, D. *Aqueous Environmental Chemistry*; Prentice-Hall Inc.: NJ, 1997.
(17) Mayes, W. M.; Jarvis, A. P.; Burke, I. T.; Walton, M.; Feigl, V.; Klebercz, O.; Gruiz, K. Dispersal and Attenuation of Trace Contaminants Downstream of the Ajka Bauxite Residue (Red Mud) Depository Failure, Hungary. *Environ. Sci. Technol.* **2011**, *45* (12), 5147−5155.
(18) Renforth, P.; Mayes, W. M.; Jarvis, A. P.; Burke; I. T.; Manning, D. A. C.; Gruiz, K. Contaminant mobility and carbon sequestration downstream of the Ajka (Hungary) red mud spill: The effects of gypsum dosing *Sci. Total Environ.* **2012**, doi: 10.1016/j.scitotenv.2012.01.046.
(19) Czovek, D.; Novak, Z.; Somlai, C.; Asztalos, T.; Tiszlavicz, L.; Bozaki, Z.; Ajtai, T.; Utry, N.; Filep, A.; Bari, F.; Petak, F. Respiratory consequences of red sludge dust inhalation in rats. *Toxicol. Lett.* **2012**, *209* (2), 113−120.
(20) USEPA. *Microwave Assisted Acid Digestion of Siliceous and Organically Based Matrices*; Method 2052; Washington DC, 1996.
(21) Saraswat, I. P.; Vajpei, A. C. Characterisation of chromium-oxide hydrate gel. *J. Mater. Sci. Lett.* **1984**, *3* (6), 515−517.
(22) Frommer, J.; Nachtegaal, M.; Czekaj, I.; Weng, T.-C.; Kretzschmar, R. X-ray Absorption and Emission Spectroscopy of Cr(III) (Hydr)Oxides: Analysis of the K-Pre-Edge Region. *J. Phys. Chem. A* **2009**, *113* (44), 12171−12178.
(23) Tomic, S.; Searle, B. G.; Wander, A.; Harrison, N. M.; Dent, A. J.; Mosselmans, J. F. W.; Inglesfield, J. E. *New Tools for the Analysis of EXAFS: The DL_EXCURV Package; CCLRC Technical Report DL-TR-2005-001*; Daresbury, UK, 2005.
(24) Binsted, N.; Hasnain, S. S. State-of-the-art analysis of whole X-ray absorption spectra. *J. Synchrotron Radiat.* **1996**, *3*, 185−196.
(25) Lowry, G. V.; Shaw, S.; Kim, C. S.; Rytuba, J. J.; Brown, G. E. Macroscopic and microscopic observations of particle-facilitated mercury transport from new idria and sulphur bank mercury mine tailings. *Environ. Sci. Technol.* **2004**, *38* (19), 5101−5111.
(26) Sherman, D. M.; Randall, S. R. Surface complexation of arsenate(V) to iron(III) (hydr)oxides: Structural mechanism from ab initio molecular geometries and EXAFS spectroscopy. *Geochim. Cosmochim. Acta* **2003**, *67* (22), 4223−4230.
(27) Shaw, S.; Pepper, S. E.; Bryan, N. D.; Livens, F. R. The kinetics and mechanisms of goethite and hematite crystallization under alkaline conditions, and in the presence of phosphate. *Am. Mineral.* **2005**, *90* (11−12), 1852−1860.
(28) Graefe, M.; Landers, M.; Tappero, R.; Austin, P.; Gan, B.; Grabsch, A.; Klauber, C. Combined Application of QEM-SEM and Hard X-ray Microscopy to Determine Mineralogical Associations and Chemical Speciation of Trace Metals. *J. Environ. Qual.* **2011**, *40* (3), 767−783.
(29) Luo, Y.; Giammar, D. E.; Huhmann, B. L.; Catalano, J. G. Speciation of selenium, arsenic, and zinc in class C fly ash. *Energy Fuels* **2011**, *25*, 2980−2987.
(30) Robins, R. G. The solubility of barium arsenate - Sherritt barium arsenate process. *Metall. Trans., B* **1985**, *16* (2), 404−406.
(31) Zhu, Y.; Zhang, X.; Xie, Q.; Chen, Y.; Wang, D.; Liang, Y.; Lu, J. Solubility and stability of barium arsenate and barium hydrogen arsenate at 25°C. *J. Hazard. Mater.* **2005**, *120* (1−3), 37−44.
(32) Wong, J.; Lytle, F. W.; Messmer, R. P.; Maylotte, D. H. K-edge absorption-spectra of selected vanadium compounds. *Phys. Rev. B* **1984**, *30* (10), 5596−5610.
(33) Sutton, S. R.; Karner, J.; Papike, J.; Delaney, J. S.; Shearer, C.; Newville, M.; Eng, P.; Rivers, M.; Dyar, M. D. Vanadium K edge XANES of synthetic and natural basaltic glasses and application to microscale oxygen barometry. *Geochim. Cosmochim. Acta* **2005**, *69* (9), 2333−2348.
(34) Chaurand, P.; Rose, J.; Briois, V.; Salome, M.; Proux, O.; Nassif, V.; Olivi, L.; Susini, J.; Hazemann, J.-L.; Bottero, J.-Y. New methodological approach for the vanadium K-edge X-ray absorption near-edge structure interpretation: Application to the speciation of vanadium in oxide phases from steel slag. *J. Phys. Chem. B* **2007**, *111* (19), 5101−5110.
(35) Chaurand, P.; Rose, J.; Briois, V.; Olivi, L.; Hazemann, J.-L.; Proux, O.; Domas, J.; Bottero, J.-Y. Environmental impacts of steel slag reused in road construction: A crystallographic and molecular (XANES) approach. *J. Hazard. Mater.* **2007**, *139* (3), 537−542.
(36) Gerke, T. L.; Scheckel, K. G.; Schock, M. R. Identification and Distribution of Vanadinite ($Pb_5(V^{5+}O_4)_3Cl$) in Lead Pipe Corrosion By-Products. *Environ. Sci. Technol.* **2009**, *43* (12), 4412−4418.
(37) Liu, R. S.; Cheng, Y. C.; Gundakaram, R.; Jang, L. Y. Crystal and electronic structures of inverse spinel-type $LiNiVO_4$. *Mater. Res. Bull.* **2001**, *36* (7−8), 1479−1486.
(38) Wehrli, B.; Stumm, W. Oxygenation of Vanadyl(IV) - Effect of coordinated surface hydroxyl-groups and OH. *Langmuir* **1988**, *4* (3), 753−758.
(39) Wehrli, B.; Stumm, W. Vanadyl in natural waters - Adsorption and hydrolysis promote oxygenation. *Geochim. Cosmochim. Acta* **1989**, *53* (1), 69−77.
(40) Wehrli, B.; Sulzberger, B.; Stumm, W. Redox processes catalysed by hydrous oxide surfaces. *Chem. Geol.* **1989**, *78* (3−4), 167−179.
(41) Hillier, S.; Lumsdon, D. G.; Brydson, R.; Paterson, E. Hydrogarnet: A host phase for Cr(VI) in chromite ore processing

residue (COPR) and other high pH wastes. *Environ. Sci. Technol.* **2007**, *41* (6), 1921−1927.
(42) Stumm, W. *Chemistry of the Solid-Water Interface*; J. Wiley: New York, 1992.
(43) Mohan, D.; Pittman, C. U. Activated carbon and low cost adsorbants for remediation of tri- and hexavalent chromium from water. *J. Hazard. Mater.* **2006**, *137*, 762−811.
(44) Arai, Y.; Elzinga, E. J.; Sparks, D. L. X-ray absorption spectroscopic investigation of arsenite and arsenate adsorption at the aluminum oxide-water interface. *J. Colloid Interface Sci.* **2001**, *235* (1), 80−88.
(45) Ladeira, A. C. Q.; Ciminelli, V. S. T.; Duarte, H. A.; Alves, M. C. M.; Ramos, A. Y. Mechanism of anion retention from EXAFS and density functional calculations: Arsenic (V) adsorbed on gibbsite. *Geochim. Cosmochim. Acta* **2001**, *65* (8), 1211−1217.
(46) Evans, H. T. Molecular structure of isopoly complex ion decavanadate ($V_{10}O_{28}^{6-}$). *Inorg. Chem.* **1966**, *5* (6), 967−977.
(47) Cornelis, G.; Poppe, S.; Van Gerven, T.; Van den Broeck, E.; Ceulemans, M.; Vandecasteele, C. Geochemical modelling of arsenic and selenium leaching in alkaline water treatment sludge from the production of non-ferrous metals. *J. Hazard. Mater.* **2008**, *159* (2−3), 271−279.
(48) Peacock, C. L.; Sherman, D. M. Vanadium(V) adsorption onto goethite (alpha-FeOOH) at pH 1.5 to 12: A surface complexation model based on ab initio molecular geometries and EXAFS spectroscopy. *Geochim. Cosmochim. Acta* **2004**, *68* (8), 1723−1733.
(49) Baes, C. F.; Mesmer, R. E. *The Hydrolysis of Cations*; John Wiley: New York, 1976.
(50) Whittleston, R. A.; Stewart, D. I.; Mortimer, R. J. G.; Tilt, Z. A.; Brown, A. P.; Geraki, K.; Burke, I. T. Chromate reduction in Fe(II)-containing soil affected by hyperalkaline leachate from chromite ore processing residue. *J. Hazard. Mater.* **2011**, *194*, 15−23.
(51) Altundogan, H. S.; Altundogan, S.; Tumen, F.; Bildik, M. Arsenic removal from aqueous solutions by adsorption on red mud. *Waste Manage.* **2000**, *20* (8), 761−767.
(52) Genc-Fuhrman, H.; Tjell, J. C.; McConchie, D. Adsorption of arsenic from water using activated neutralized red mud. *Environ. Sci. Technol.* **2004**, *38* (8), 2428−2434.
(53) Rajapaksha, A. U.; Vithanage, M.; Jayarathna, L.; Kumara, C. K., Natural Red Earth as a low cost material for arsenic removal: Kinetics and the effect of competing ions. *Appl. Geochem.* **2011**, *26* (4), 648−654.
(54) Manning, B. A.; Goldberg, S. Modeling competitive adsorption of arsenate with phosphate and molybdate on oxide minerals. *Soil Sci. Soc. Am. J.* **1996**, *60* (1), 121−131.
(55) Genc, H.; Tjell, J. C.; McConchie, D.; Schuiling, O. Adsorption of arsenate from water using neutralized red mud. *J. Colloid Interface Sci.* **2003**, *264* (2), 327−334.
(56) Islam, F. S.; Gault, A. G.; Boothman, C.; Polya, D. A.; Charnock, J. M.; Chatterjee, D.; Lloyd, J. R. Role of metal-reducing bacteria in arsenic release from Bengal delta sediments. *Nature* **2004**, *430* (6995), 68−71.